Performance Analysis of a Wireless Backhaul in a Three-Tier Hybrid Network With Directional Antennas

HEBATALLAH SHOUKRY[ID][1], **NAVEEN MYSORE BALASUBRAMANYA**[ID][2], **(Member, IEEE),**
SATYANARAYANA VUPPALA[3], **(Member, IEEE),**
AND MATHINI SELLATHURAI[1], **(Senior Member, IEEE)**
[1]Institute Sensors, Signals, and Systems, Heriot-Watt University, Edinburgh EH14 4AS, U.K.
[2]Department of Electrical Engineering, IIT Dharwad, Dharwad 580011, India
[3]United Technologies Research Center, Cork T23 XN53, Ireland
Corresponding author: Hebatallah Shoukry (hs33@hw.ac.uk)

ABSTRACT In this paper, a three-tier hybrid cellular heterogeneous network is considered using the microwave (μWave) links for the first two tiers and millimeter (mmWave) links for the last tier. The two-tiers with μWave links form a wireless backhaul to the last tier with mmWave links. The main challenge in having a wireless backhaul is to suppress interference. Thus, we propose a novel and practical model where we can reuse the μWave infrastructure, but equip the BSs with directional antennas to have a robust wireless backhaul network. To solve the bottleneck rate problem, we assume that the rate required by the mmWave users is comparable to that offered by the μWave links. Different configurations based on the placement of the directional antennas at each tier are explored. The analysis of the key performance indicators, namely, the coverage probability, area spectral efficiency, and energy efficiency using the conventional minimum rate model, and the simulation results associated with these parameters are presented. In order to analyze this hybrid network with a wireless backhaul, an optimization problem for the overall area spectral efficiency and energy efficiency with respect to the optimal signal-to-interference ratio (SIR) threshold required for μWave and mmWave links is investigated. Results indicate that the optimal SIR threshold required for the μWave tiers (wireless backhaul) depends only on the path-loss exponent and that for the mmWave tier depends on the area of the line-of-sight region. Finally, instead of the conventional minimum rate model, we consider the average rate under coverage and show that the area spectral efficiency and energy efficiency are strictly decreasing functions with respect to the threshold, thereby concluding that they can be maximized by choosing the lowest possible SIR threshold available in the system.

INDEX TERMS Directional antennas, heterogeneous networks, stochastic geometry, wireless backhaul.

I. INTRODUCTION

Heterogeneous networks (HetNets) incorporating a layered structure of macrocells, femtocells, and/or picocells are deployed to offer improved wireless coverage in various scenarios ranging from open outdoor environments to office buildings, homes and underground areas. Apart from improved coverage, there are several benefits to Het-Nets as opposed to a traditional homogeneous wireless networks including increased reliability and improved spectrum efficiency [1]–[6]. While the coverage and reliability improve

The associate editor coordinating the review of this manuscript and approving it for publication was Bora Onat.

because the base-stations (BSs) in one tier can fill the coverage holes of other tiers and maintain a connection, spectral efficiency is enhanced because of better load balancing of users across BSs from different tiers.

A key result from early HetNet analysis is the derivation of the signal-to-interference-plus-noise ratio (SINR) distribution which is then mapped to the coverage probability [1], [2]. A favorable property of HetNets was shown in [5] and [6], which stated that the distribution of the SINR is invariant to the network density, as long as all tiers have the same threshold. Thus, the area spectral efficiency (ASE) of the HetNet can be increased by deploying more BSs. A higher ASE means that more users can be supported by the network

with a higher spatial reuse efficiency. However, the dense and random deployment of small cells raised questions about the energy efficiency (EE) implications. To this end in [4], active/sleep (on/off) modes were introduced for BSs, leading to improved EE. Another solution based on the joint maximization of EE and spectral efficiency while ensuring proportional rate fairness among users and taking into account the backhaul capacity constraint was analyzed in [7].

The aforementioned performance metrics are analyzed using the tools of stochastic geometry, mainly point process theory [1]–[6]. For example, a tractable and flexible model for a downlink HetNet of K tiers was presented in [2]. Assuming that a mobile connects to the strongest BS, the probability of coverage as well as the average rate under coverage achieved by a randomly located mobile were derived. In [3], a framework for the uplink ASE analysis in case of a multi-channel HetNet was developed using a biased cell association scheme with coordinated sub-channel allocation and channel inversion power control for mitigating the interference. In [4], based on the stochastic geometry model, the success probability and EE were derived for homogeneous single tier and heterogeneous K-tier wireless networks under different sleeping policies. It was also shown that the deployment of small cells generally leads to higher EE but this gain saturates as the density of small cells increases.

While [1]–[6] focused on microwave (μWave) HetNets, millimeter wave (mmWave) communication has emerged as a key enabler for higher spectral efficiency and EE in the fifth generation (5G) wireless communication networks. Unlike μWave, they operate at 10 to 300 GHz frequency bands with available bandwidths of 2 GHz or more [8]–[13]. A general framework to evaluate coverage and a tractable model for rate performance were proposed in [11] and [12], where it was shown that dense mmWave networks can achieve comparable coverage and much higher data rates than conventional ultra high frequency (UHF) cellular systems, despite the presence of blockages.

Recently, because of the advantages of μWave and mmWave communications, hybrid networks consisting of a HetNet with μWave and mmWave tiers were introduced [14]–[16]. In [14], the performance in terms of coverage and rate of hybrid cellular networks consisting of BSs operating at mmWave and sub 6 GHz bands was investigated. The results showed that the hybrid network achieved an average rate under coverage which is comparable to that of a mmWave network and much higher than the stand alone UHF network. In [15], the downlink performance in terms of coverage and rate of a three tier hybrid network where massive multiple input multiple output (MIMO) macro base stations (MBSs) are overlaid with small cells operating at either sub 6 GHz or mmWave bands was presented and the users were assumed to connect to any of the tier according to the association probability. It was observed that the implementation of massive MIMO on macro tier and deployment of high density of mmWave small cells led to the enhancement of rate and coverage. Similar system model was presented in [16], but

the MBSs were not equipped with massive MIMO, and the effects of BS density on ASE and EE were studied. Based on the analysis, introducing mmWave small cells considerably improved coverage and hence ASE, and EE.

A. MOTIVATION

We consider the system model of the three tier hybrid network similar to [16] which consists of small cells overlaid with macrocells. However, in our model the user terminals can only communicate to mmWave tier and have no direct access links to the μWave tiers. We assume that the rate required by the mmWave users is compared to that offered by the μWave links. In previous works [14]–[16], the end-users were assumed to have the ability to operate in μWave or mmWave, which implies that the user's radio equipment operates over a wide frequency range. Practically, this assumption increases the cost of end-user's equipment. Therefore, we considered the scenario where end-users have mmWave equipment only and hence can connect to the last tier. Moreover, we use the μWave links as the wireless backhaul to the mmWave users.

Wireless backhaul recently gained a lot of attention in multi-tier networks to overcome the expensive cost of wired backhaul architecture and the installation difficulty [17]–[24]. One of the main challenges in having a wireless backhaul is to mitigate interference. The proposed methods in [22]–[24] tried to reduce the interference, but required additional infrastructure that led to increased expenditure. This motivated us to propose a novel and practical model where we can reuse the μWave infrastructure, but equip the BSs with directional antennas to have a robust wireless backhaul network. The use of directional antennas not only suppresses interference, but also leads to lower system complexity as discussed later in Section IV.

B. CONTRIBUTIONS

The main contributions of this paper are as follows:

- We present a tractable stochastic geometric approach to perform the analysis of the downlink three-tier hybrid cellular HetNet using μWave links for the first two tiers and mmWave links for the last tier. We examine the impact of the usage of directional antennas for the wireless backhaul network, and analyse the performance of the considered network in terms of coverage probability, ASE and EE using the conventional minimum rate model.

- We formulate an optimization problem to find the optimal signal-to-interference ratio (SIR) threshold that maximizes the ASE and EE for the entire network. Our system model enables us to separate this problem into two independent subproblems corresponding to μWave backhaul link and mmWave user links, respectively. We show that the ASE and EE optimization problems of the wireless backhaul HetNet results in an optimum solution that is only dependent on the path-loss exponent

of the μWave network. Unfortunately, the optimzation problem for the mmWave communications is not analytically tractable. Therefore, the optimal SIR threshold is evaluated numerically and an analytical plot for the ASE of the mmWave link with respect to different SIR thresholds is presented. For both subproblems, we use Monte-Carlo simulations to demonstrate the proximity of our analytical results with the experimental ones.

- We also analyze the ASE and EE for the μWave link considering the average rate under coverage. The average rate under coverage refers to the average rate achieved by the picocells conditioned that they are covered, i.e., the received SIR is greater than a predefined threshold. This metric is greater than minimum rate and closer to the rate observed in practical deployments. Moreover, we will show that using the average rate under coverage, ASE and EE will be strictly decreasing functions and are maximized by choosing the lowest possible SIR threshold in the system. Furthermore, since we use μWave link as the wireless backhaul, we analyze its average rate under coverage separately in order to determine its suitability as a reliable wireless backhaul.

This paper is organized as follows. Section II presents the system model considered in this work. Section III demonstrates the performance analysis of the wireless backhaul μWave two tier network as well as the mmWave tier in terms of minimum rate model, and the associated optimization problems. In Section IV, the numerical and simulation results are presented and we analyze the μWave link in terms of average rate under coverage in Section V. Conclusions are stated in Section VI.

II. SYSTEM MODEL

In this section, we define our system model for the performance analysis of the hybrid HetNet. We focus on evaluating a two tier μWave network as a wireless backhaul network for a non-dense mmWave network in terms of coverage, rate under coverage, ASE and EE. The system model is shown in Fig. 1. The mathematical formulation and the underlying assumptions are discussed in the following subsections.

A. POISSON POINT PROCESS (PPP) BSS AND USERS

The μWave tier consists of macrocell base stations (MBSs) and femtocell base stations (FBSs) and the mmWave tier consists of picocell base stations (pBSs). Each tier of the HetNet is modelled as an independent Poisson Point Process (PPP) Φ_k with density λ_k, where $k \in \{m, f, w\}$ indicating macro, femto and pico tiers, respectively. All base stations (femto and macro) are considered to operate in open access. Open access refers to the scenario that a typical pBS is allowed to connect to base stations from any μWave tier [2]. The decision criteria on whether to connect to a MBS or to a FBS will be discussed in more detail in Section III.

The end-users, referred by the term user equipments (UEs), are also modelled as a PPP Φ_u with density λ_u. The UEs
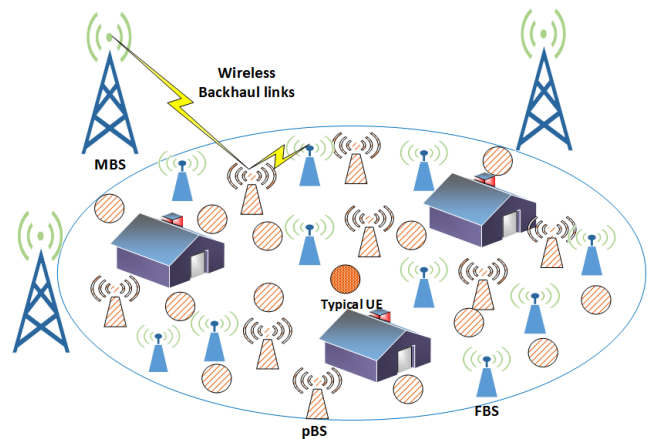
FIGURE 1. A three-tier hybrid cellular heterogeneous network (HetNet) using μWave links (wireless backhaul links) for the first two tiers and mmWave links for the last tier.

only communicate with pBSs in the mmWave band. In other words, the pBSs relay the information from the first two tiers (μWave) to the UEs. It is assumed that the rate required by the mmWave UE is comparable to that offered by the μWave links.

B. DIRECTIONAL BEAMFORMING MODELING

For μWave and mmWave tiers, all directional antennas are approximated by a sectored antenna model which renders the analysis tractable [11]. In the sectored antenna model, antenna gains are assumed to be constant M for all angles within the beamwidth of the main lobe, and another constant S otherwise. Mathematically, the antenna gain (transmit/receive) is given as

$$G_{T/R}(\theta) = \begin{cases} M_{T/R} & \text{if } |\theta_{T/R}| \leq \theta_M \\ S_{T/R} & \text{otherwise,} \end{cases} \quad (1)$$

where T is the transmitter and R is the receiver, $\theta_{T/R}$ is the transmit/receive angle of antenna directivity and θ_M is the beamwidth of the main lobe width for the directional antenna.

For both transmit and receive nodes equipped with directional antennas, we assume that the desired and typical nodes are perfectly aligned. Then for the desired link, $G_{\max} = M_T M_R$, but for other interfering links, θ_T and θ_R are assumed to be independent and uniformly distributed in $(0, 2\pi]$, which results in a random directivity gain G_{int}. Therefore, the directivity gain in an interference link G_{int} is a discrete random variable, as shown in (2)

$$G_{\text{int}} = \begin{cases} M_T M_R & p_{MM} = \left(\dfrac{\theta_T}{2\pi}\right)\left(\dfrac{\theta_R}{2\pi}\right) \\ M_T S_R & p_{MS} = \left(\dfrac{\theta_T}{2\pi}\right)\left(\dfrac{2\pi - \theta_R}{2\pi}\right) \\ S_T M_R & p_{SM} = \left(\dfrac{2\pi - \theta_T}{2\pi}\right)\left(\dfrac{\theta_R}{2\pi}\right) \\ S_T S_R & p_{SS} = \left(\dfrac{2\pi - \theta_T}{2\pi}\right)\left(\dfrac{2\pi - \theta_R}{2\pi}\right), \end{cases} \quad (2)$$

However if the transmitter node is equipped with omni directional antenna, then its antenna directivity gain would be unity and the total antenna directivity gain for the desired link is $G_{\max} = M_R$. The total antenna directivity for the interfering links reduces to

$$
G_{\text{int}} = \begin{cases} M_R, & \text{with } p_M = \dfrac{\theta_R}{2\pi} \\ S_R, & \text{with } p_S = \dfrac{2\pi - \theta_R}{2\pi} \end{cases} \tag{3}
$$

C. LINE-OF-SIGHT (LOS) BS AND PATH-LOSS MODEL FOR mmWave LINKS

Let the length of the mmWave link between p^{th} BS and the typical UE be denoted by D_w. Since the distribution of blockages is stationary and isotropic, the probability that the link is line-of-sight (LOS), indicated by p_L, only depends on the link length D_w [25]. Considering the LOS area to be within a circular ball of radius r_w centered around the pBS location (where r_w denotes the maximum distance for LOS communication), we get

$$
p_L = \begin{cases} 1 & \text{if } D_w \le r_w \\ 0 & \text{otherwise.} \end{cases} \tag{4}
$$

Since the LOS and non-line-of-sight (NLOS) probabilities are complementary, the NLOS probability $p_N = 1 - p_L$. Different path-loss laws apply to LOS and NLOS links. Given a link length D_w between intended p^{th} BS and typical mmWave UE, the path-loss value $L(D_w)$ can be computed as in [11].

D. SMALL-SCALE FADING

We assume independent small-scale Rayleigh fading channels[1] Ψ_k where $k \in \{f, m, w\}$, with β as the path-loss exponent for the two μWave links. But in mmWave networks, measurements have shown difference between the path-loss exponents for LOS and NLOS links [11]. Therefore, the path-loss exponents in mmWave links are α_L and α_N, for LOS and NLOS, respectively. Due to the thinning property in stochastic geometry [27], the density of pBSs Φ_w can be split into two marked PPPs Φ_w^L with density $p_L \lambda_w$ and Φ_w^N with density $(1 - p_L)\lambda_w$. All notations are listed in Table 1.

E. SINR MODELING:

1) μWAVE TIERS

Using Slivnyak's theorem [28], we assume that the receiver for the first two μWave tiers, the typical pBS, is located at the origin. The received SINR of the typical pBS at a distance D_j associated with its jth tier BS, for $j \in \{m, f\}$ can be expressed as

$$
\zeta_\mu^j = \frac{P_T^j |h_0^j|^2 G_{\max}^j D_j^{-\beta}}{\sigma^2 + \sum\limits_{j \in \{m,f\}} \sum\limits_{i \in \Phi_j \backslash 0} P_T^j |h_i^j|^2 G_{\text{int}_i}^j r_i^{-\beta}} \tag{5}
$$

where the notations and descriptions are given in Table 1.

[1] Small scale fading on mmWave networks is applicable for some particular cases of mmWave networks [26].

TABLE 1. Notations.

Notation	Description
P_T^k	Transmit power, where $k \in \{m, f, w\}$
Φ_k	PPP, where $k \in \{m, f, w\}$
D_j	Intended link length between j^{th} BS and typical pBS, where $j \in \{m, f\}$
D_w	Intended link length between p^{th} BS and typical mmWave UE
β	Path-loss exponent of μWave tiers
α_L	LOS path-loss exponent for pBSs (mmWave tier)
α_N	NLOS path-loss exponent for pBSs (mmWave tier)
p_L	LOS probability
r_i	Distance from the interferer i to the typical pBS
h_0^k	Desired fading channel, where $k \in \{m, f, w\}$
h_i^k	Interference fading channel, where $k \in \{m, f, w\}$
$G_{\max}^k$	Maximum (assuming perfect alignment) distributed directivity gain (DDG), where $k \in \{m, f, w\}$
G_{int}^k	Interfering (non-intended links) DDG, where $k \in \{m, f, w\}$
ζ_μ	Received SINR from μWave tiers
ζ_w	Received SINR from mmWave tier
σ^2	Thermal noise
r_w	Radius of LOS region in mmWave tier

2) mmWave TIER

μWave and mmWave tiers are independent, therefore, we can apply Slivynak's theorem to the last tier by considering a typical UE at the origin. Thus, the received SINR of a typical UE at distance D_w from pBSs can be expressed as

$$
\zeta_w = \frac{P_T^w |h_0^w|^2 G_{\max}^w L(D_w)}{\sigma^2 + \sum\limits_{z \in \{L,N\}} \sum\limits_{y \in \Phi_w^z \backslash 0} P_T^w |h_y^w|^2 G_{\text{int}_y}^w L(r_y)} \tag{6}
$$

where $L(r_y)$ is the path loss value with respect to the interfering pBSs and $L(D_w)$ is defined in Section II-C. The rest of the notations and definitions are given in Table 1.

III. PERFORMANCE ANALYSIS FOR μWAVE AND mmWave TIERS

In this section, we analyze the coverage probability, ASE and EE in the proposed system using the stochastic geometry tools. For the μWave tier, pBSs are considered as receivers and for the mmWave tier, the UEs are considered as receivers. Directional antennas are equipped at the μWave tiers to increase SINR and hence improve the coverage. The coverage probability is referred to the probability that the received SINR is bigger than a required threshold and it is considered as the base building block for the analysis of all other parameters such as average rate, ASE and EE [1], [3]. ASE can be quantified as the total rate in unit area normalized by the bandwidth. EE can be measured as the ratio of the area spectral efficiency to the average network power consumption. In this section, we consider the minimum average rate model for both μWave and mmWave tiers [29], [30]. Our objective is to find the optimal SINR threshold that maximizes ASE and EE.

A. COVERAGE PROBABILITIES $\mathcal{P}_\mu^c$ AND $\mathcal{P}_w^c$

1) μWAVE TIER COVERAGE PROBABILITY $\mathcal{P}_\mu^c$

For the rest of the μWave analysis, we consider SIR instead of SINR. This is because it was shown in [2, Sec. V] that in multi tier HetNets, self-interference dominates thermal noise. Hence, thermal noise has a very limited effect on the coverage probability of multi tier HetNets. We consider instantaneous SIR based scheme [4], where the pBS connects to the μWave tier j if the instantaneous SIR exceeds γ_j, where $j = \{m, f\}$. In the case where both tiers have a connection with the typical pBS, then this typical pBS is covered by the tier with the highest SIR. We assume that the pBS can connect to at most one tier and that $\gamma_j > 1$ [2].

a: MODEL CONFIGURATION

The considered system model is evaluated under four different configurations according to the type of antenna and its placement at FBS and pBS, as shown in Table 2. The MBSs always use an omnidirectional antenna and the UEs always employ a directional antenna for all the configurations. Evaluating different configurations enables us to show the effect of adding directional antenna at one or more tiers to improve the performance of the considered network.

TABLE 2. Antenna configurations for different models.

BS Type \ Model	1	2	3	4
FBS	Omni	Directional	Omni	Directional
pBS	Omni	Omni	Directional	Directional

Proposition 1: Following the model in [31], the analytical coverage probability for directional antenna used at different tiers can be derived as

$$\mathcal{P}_\mu^c = \frac{\pi}{C(\beta)} \frac{\sum_{j\in\{m,f\}} \lambda_j (P_T^j G_{\max}^j)^{2/\beta} \gamma_j^{-2/\beta}}{\sum_{j\in\{m,f\}} \lambda_j (P_T^j G_{\min}^j)^{2/\beta}}, \quad (7)$$

where $C(\beta) = \frac{2\pi^2}{\beta}\csc(\frac{2\pi}{\beta})$, $\csc(.) = \frac{1}{\sin(.)}$, $G_{\min}^j$ is the average interfering directivity gains, where $G_{\min}^f = \sum p_{lk}(l_T k_R)$ where $l, k \in \{M, S\}$, and $G_{\min}^m = p_M M + p_S S$.

The proof is given in details in Appendix A.

The total coverage probability can be calculated as the sum of all the individual coverage probabilities of all tiers given that $\gamma_j > 1$ [2]:

$$\mathcal{P}_\mu^c = \mathcal{P}_m^c + \mathcal{P}_f^c, \quad (8)$$

Our system model is based on the assumption that the probabilities of different tiers are mutually exclusive,.i.e., if $\mathcal{P}_{c_m} = 1$, then $\mathcal{P}_{c_f} = 0$. Then, the individual coverage probabilities are given as

$$\mathcal{P}_f^c = \frac{\pi}{C(\beta)} \frac{\lambda_f (P_T^f G_{\max}^f)^{2/\beta} \gamma_f^{-2/\beta}}{\sum_{j\in\{m,f\}} \lambda_j (P_T^j G_{\min}^j)^{2/\beta}}, \quad (9a)$$

$$\mathcal{P}_m^c = \frac{\pi}{C(\beta)} \frac{\lambda_m (P_T^m G_{\max}^m)^{2/\beta} \gamma_m^{-2/\beta}}{\sum_{j\in\{m,f\}} \lambda_j (P_T^j G_{\min}^j)^{2/\beta}}, \quad (9b)$$

2) mmWave TIER COVERAGE PROBABILITY $\mathcal{P}_w^c$

For the mmWave analysis, unlike the μWave analysis, we consider SINR threshold. Because mmWave is a single tier and we assume non-dense network, therefore the thermal noise can not be ignored [11]. Hence, the coverage probability for the mmWave links (UEs) based on the highest received SINR is analysed. We consider the UE to be covered by the pBS with the highest SINR [30]. Note that in mmWave networks, different path-loss laws are applied to LOS and NLOS links [10], [32].

Proposition 2: The total coverage probability of the mmWave tier, $\mathcal{P}_w^c$, is given by

$$\mathcal{P}_w^c = \mathcal{P}_L^c + \mathcal{P}_N^c, \quad (10)$$

where $\mathcal{P}_L^c$ and $\mathcal{P}_N^c$ are the LOS, and NLOS coverage probabilities, respectively.

The LOS and NLOS coverage probabilities $\mathcal{P}_L^c, \mathcal{P}_N^c$ can be written mathematically as,

$$\mathcal{P}_L^c = e^{-s_L - 2\pi\lambda_w\Theta_1} \quad (11a)$$

$$\mathcal{P}_N^c = e^{-s_N - 2\pi\lambda_w\Theta_2} \quad (11b)$$

respectively,
where

$$s_L = \frac{\gamma_w r_w^{\alpha_L}\sigma^2}{P_T^w G_{\max}^w}, \quad s_N = \frac{\gamma_w r_w^{\alpha_N}\sigma^2}{P_T^w G_{\max}^w}, \quad (12a)$$

$$\Theta_1 = \left[p_L \int_0^{r_w} \frac{y}{1+s_1^{-1}y^{\alpha_L}}dy + p_N \int_0^{r_w} \frac{z}{1+s_1^{-1}z^{\alpha_N}}dz \right], \quad (12b)$$

$$\Theta_2 = \left[p_L \int_{r_w}^{\infty} \frac{y}{1+s_2^{-1}y^{\alpha_L}}dy + p_N \int_{r_w}^{\infty} \frac{z}{1+s_2^{-1}z^{\alpha_N}}dz \right], \quad (12c)$$

$$s_1 = \frac{\gamma_w r_w^{\alpha_L} G_{\min}^w}{G_{\max}^w}, \quad s_2 = \frac{\gamma_w r_w^{\alpha_N} G_{\min}^w}{G_{\max}^w}. \quad (12d)$$

where p_L and p_N are defined in Section II-C, $G_{\max}^w$ and $G_{\min}^w$ are the maximum and minimum antenna directivity gains, respectively, that can be calculated as described in Section II-B and Proposition 1. The rest of the notations are defined in Table 1.

The proof is stated in Appendix B.

B. AVERAGE RATES R_μ AND R_w

In literature, typically the minimum rate model is used for μWave tiers, which is $R_\mu = \log_2(1 + \gamma_\mu)$, where $\gamma_\mu = \gamma_m = \gamma_f$ is the predefined threshold common to all the μWave tiers [29]. Furthermore, the mmWave is a single tier with a single threshold γ_w, that is the same for LOS and NLOS pBSs. Therefore, the minimum rate achieved by the typical UE depends only on the required threshold γ_w is given by [33]

$$R_w = \log_2(1 + \gamma_w). \quad (13)$$

C. ASE η AND EE Ω OPTIMIZATION

Our objective is to find the optimal threshold for the considered system model that maximizes ASE and EE. Because the μWave and mmWave tiers operate at different frequencies, they are considered independent. Thus, the overall ASE η_{tot} and EE Ω_{tot} for the three tier hybrid cellular network are the sum of these metrics for each tier. Mathematically,

$$\eta_{\text{tot}} = \sum_{j \in \{m,f\}} \lambda_j \mathcal{P}_j^c(\gamma_\mu) R_\mu + \lambda_w \mathcal{P}_w^c(\gamma_w) R_w, \quad (14a)$$

$$\Omega_{\text{tot}} = \frac{\sum_{j \in \{m,f\}} \lambda_j \mathcal{P}_j^c(\gamma_\mu) R_\mu + \lambda_w \mathcal{P}_w^c(\gamma_w) R_w}{\sum_{j \in \{m,f\}} \lambda_j (P_{j0} + \Delta_j P_j) + \lambda_w (P_{w0} + \Delta_w P_w)}, \quad (14b)$$

where P_{k0} is the static power, P_k is the RF output power, and Δ_k is the slope of load-dependent power consumption [34], for $k \in \{f, m, w\}$, indicating femto, macro and pico tiers.

Since we assume here that the density is fixed, the optimization is with respect to the SIR threshold. The threshold not only affects the coverage probability (which implies that the transmission links are reliable), but also the rate at which the nodes are communicating. Moreover, since the μWave tiers operate as wireless backhaul to the mmWave tier, the rate of backhaul transmissions in μWave tiers should be greater than the rate of access transmissions in mmWave tier. Therefore the overall optimization problems for the ASE and EE are given as

$$\underset{\gamma_\mu, \gamma_w}{\text{maximize}} \ \eta_{\text{tot}},$$
$$\text{subject to } R_\mu > R_w, \quad (15)$$

$$\underset{\gamma_\mu, \gamma_w}{\text{maximize}} \ \Omega_{\text{tot}},$$
$$\text{subject to } R_\mu > R_w, \quad (16)$$

Considering that the μWave and mmWave tiers operate at different frequencies and the two tiers are independent, the overall optimization problem can be split into two independent problems as shown in the following.[2]

1) μWAVE TIER

In order to find the optimal SIR threshold that maximizes the ASE for the μWave tier, the optimization problem is stated as in (15), where the constraint insures higher data rate for wireless backhaul information than access information [23].

The solution to the optimization problem (15) is shown in the proof of the following Proposition.

Proposition 3: The optimal threshold γ_μ^* of μWave tier to obtain the maximum ASE η_μ is only dependent on the path-loss exponent β of the μWave tier,

$$\gamma_\mu^* = e^{\xi^*} - 1, \quad (17)$$

where $\xi^* = \dfrac{a * W(-\dfrac{e^{-1/a}}{a}) + 1}{a}$, $a = 2/\beta$, and $W(.)$ is the Lambert Function.

Proof: The optimization problem can be formulated as the following:

$$\underset{\gamma_\mu, \gamma_w}{\text{maximize}} \ \left[\lambda_f \mathcal{P}_f^c(\gamma_\mu) + \lambda_m \mathcal{P}_m^c(\gamma_\mu) \right]$$
$$\times \log_2(1 + \gamma_\mu) + \lambda_w \mathcal{P}_w^c(\gamma_w) R_w,$$
$$\text{subject to } \log_2(1 + \gamma_\mu) > \log_2(1 + \gamma_w), \quad (18)$$

or as an equivalent problem,

$$\underset{\gamma_\mu, \gamma_w}{\text{maximize}} \ \left[\lambda_f \mathcal{P}_f^c(\gamma_\mu) + \lambda_m \mathcal{P}_m^c(\gamma_\mu) \right]$$
$$\log_2(1 + \gamma_\mu) + \lambda_w \mathcal{P}_w^c(\gamma_w) R_w,$$
$$\text{subject to } \gamma_\mu > \gamma_w. \quad (19)$$

To solve this problem, we first assume a fixed value for $\gamma_w = \gamma_w^{th}$ and the final optimization problem is given as

$$\underset{\gamma_\mu^*}{\text{maximize}} \ \left[\lambda_f \mathcal{P}_f^c(\gamma_\mu) + \lambda_m \mathcal{P}_m^c(\gamma_\mu) \right]$$
$$\times \log_2(1 + \gamma_\mu) + \eta_w,$$
$$\text{subject to } \gamma_\mu > \gamma_w^{th}. \quad (20)$$

Using the Lagrangian function [35], we get

$$\mathbb{L}(\gamma_\mu) = -\left[\lambda_f \mathcal{P}_f^c(\gamma_\mu) + \lambda_m \mathcal{P}_m^c(\gamma_\mu) \right] \log_2(1 + \gamma_\mu)$$
$$- \eta_w - \epsilon_1 [\gamma_\mu - \gamma_w^{th}], \quad (21)$$

where ϵ_1 is the Lagrange multiplier. The derivative of the Lagrangian function with respect to γ_μ is computed as:

$$\frac{\partial \mathbb{L}}{\partial \gamma_\mu} = \frac{\gamma_\mu}{1 + \gamma_\mu} - \frac{2}{\beta} \ln(1 + \gamma_\mu) - \epsilon_1. \quad (22)$$

Using the Karush-Kuhn-Tucker (KKT) conditions [35], and in particular the complementary slackness condition, $\epsilon_1(\gamma_\mu - \gamma_w^{th}) = 0$ and applying a change of variable, i.e., setting $\ln(1 + \gamma_\mu) = \S$, the optimal solution can be found as

$$\xi^* = \frac{a * W(-\dfrac{e^{-1/a}}{a}) + 1}{a}, \quad (23)$$

where $a = 2/\beta$, and $W(.)$ is the Lambert Function. Therefore, $\gamma_\mu^* = e^{(\xi^*)} - 1$, which shows that the optimal SIR threshold γ_μ^* only depends on the path-loss exponent β.
This concludes the proof. ☐

2) mmWave TIER

We need to find the optimal SINR threshold for mmWave BSs (γ_w) that maximizes the ASE with the threshold of the μWave tiers fixed as γ_μ^{th}. To this end, we define a new optimization problem,

$$\underset{\gamma_w^*}{\text{maximize}} \ \eta_\mu + \lambda_w \mathcal{P}_w^c(\gamma_w) R_w,$$
$$\text{subject to } \gamma_w < \gamma_\mu^{th}. \quad (24)$$

---

[2]Please note that we present the analysis for ASE only. This is because both EE and ASE are related by a constant (power consumption) which is independent of the required threshold. However, in the results section we present both metrics.

The Lagrangian function is given by

$$\mathbb{L}(\gamma_w) = -(\eta_\mu + \lambda_w \mathcal{P}_w^c(\gamma_w) R_w) + \epsilon_2[\gamma_w - \gamma_\mu^{th}], \quad (25)$$

where ϵ_2 is the Lagrange multiplier. The optimal SINR threshold can be computed by differentiating (25) with respect to γ_w, and equating the result to zero.

The integrals in (12) can be computed as

$$\int \frac{y}{1 + s_1^{-1} y^{\alpha_L}} dy = \frac{s_1}{2} \log_2(|1 + s_1^{-1} r_w^2|), \quad (26a)$$

$$\int \frac{z}{1 + s_1^{-1} z^{\alpha_N}} dz = \frac{1}{2} r_w^2 \, {}_2F_1(a_N, b; c; T_1), \quad (26b)$$

$$\int \frac{y}{1 + s_2^{-1} y^{\alpha_L}} dy = \frac{s_2}{2} \log_2(|1 + s_2^{-1} r_w^2|), \quad (26c)$$

$$\int \frac{z}{1 + s_2^{-1} z^{\alpha_N}} dz = \frac{1}{2} r_w^2 \, {}_2F_1(a_N, b; c; T_2), \quad (26d)$$

where $\alpha_L = 2$, $\alpha_N \neq 2$, ${}_2F_1(a_N, b; c; T)$ is the Hypergeometric function and $a_N = 2/\alpha_N$, $b = 1$, $c = a_N + 1$, $T_1 = -s_1^{-1} r_w^{\alpha_N}$ and $T_2 = -s_2^{-1} r_w^{\alpha_N}$, where s_1 and s_2 were defined in Proposition 2. Unfortunately, this problem is not analytically tractable. Therefore, we only show a plot of different SINR thresholds and their corresponding ASE in Section IV.

IV. RESULTS

In this section, we compare the numerical results derived in Section III with the experimental results obtained using Monte-Carlo simulations. The values for the parameters used in simulation and analytical results are specified in Table 3. The coverage probability plots have the same behaviour to the work presented in [2] and [16]. For ASE plots, similar curves have been obtained in [3] but for different system model and settings. The EE results are expected to behave as ASE, since both are related by a constant (power consumption) which is independent of the required threshold.

TABLE 3. The values for parameters used in simulation and analytical results [2], [12].

Parameter	Value	Parameter	Value
total area	$4 \ km^2$	P_t^f	30 dBm
λ_m	$2 \ /km^2$	P_t^m	46 dBm
λ_f	$50\lambda_m$	r_w	100 m or 150 m
λ_w	$100 \ /km^2$	N_0	-117 dBm/Hz
β	3	α_w^N	3.3
α_w^L	2	P_t^w	30 dBm

As mentioned in Section III-A1a, the model configurations presented in Table 2 enables us to show the effect of adding directional antenna at one or more tiers to improve the performance of the considered network. For example, in Model 2 when the directional antenna is deployed at the FBSs only (assuming a random direction for the beam), we expect that the performance will be slightly better than Model 1. This is because in Model 1, all BSs use omnidirectional antennas, which increases the interference signal

received by the typical pBS, leading to reduced SIR and hence reduced coverage probability. However in Model 2, the use of directional antennas at FBSs results in lower interference to the typical pBS. In Model 3, directional antenna at the typical pBS receiver ensures that the amount of interference received is limited to the angular spread of the main lobe of the antenna. This in-turn increases the SIR and hence results in improved coverage. Similarly, further improvement can be obtained using Model 4 where both FBSs and pBS have directional antennas. Since in Models 1 and 2 (3 and 4) pBSs are equipped with omnidirectional (directional) antennas, respectively, we expect the results to be close results for Models 1 and 2 (3 and 4).

It should be noted that although employing directional antennas improves performance, it incurs additional cost. Especially, in Model 3, directional antennas, for μWave and mmWave communication, equipped at the pBS cause more complexity, which would result in a physically unrealizable scenario. Hence, there is a trade-off between the cost and performance. To this end, we advocate the use of electronically steerable parasitic antenna radiator (ESPAR) as the directional antenna for the μWave communication.[3] As a result, Model 3 is indeed physically realizable.

The ESPAR is a parasitic antenna that uses a single RF chain to transmit and receive data, and as such is a practical solution to the constraints of size, power, weight and cost on a variety of radio equipment [36]. Furthermore, the antenna system requires mutual coupling between the active and parasitic elements; this requires closely spaced antenna elements, which makes the ESPAR antenna suitable for small mobile equipment applications, such as pBSs as stated in our problem. The ESPAR antennas have been studied for a variety of applications [37]–[42].

The antenna directivity gains for the ESPAR in simulation results are calculated by considering a low-complexity approach where the ESPAR works as a switched-beam antenna capable of predefining directional beampatterns accessing to different angle sectors [37], [40]. These beampatterns are controlled by adjusting a few tuneable loads of parasitic elements [39].

However, for the analytical results, we do not use it as a switched beam antenna and choose the values for the maximum and average directivity gains approximately using the beam pattern in one particular direction. Hence, there is a small difference between simulation and analytical results for the directional antennas.

A. μWAVE TIERS
In Fig. 2a, and 2b, the coverage probability of the μWave is plotted with respect to the SIR threshold γ_μ comparing all four Models in Table 2. First from Fig. 2a, we observe that Model 4 outperforms Model 1, resulting in higher coverage probability (almost double) at the typical pBS, as expected.

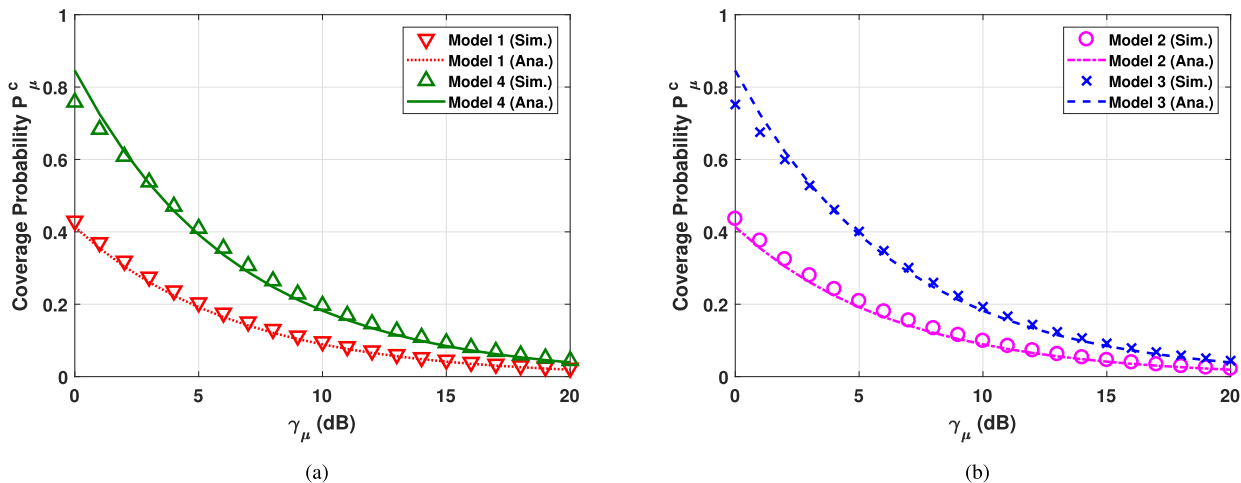[3]Note that our performance analysis holds for any sectored directional antenna

FIGURE 2. The coverage probability ($\mathcal{P}[SIR > \gamma_\mu]$) of μWave tiers for different SIR thresholds γ_μ. (a) Coverage Probability for Models 1 and 4. (b) Coverage Probability for Models 2 and 3.

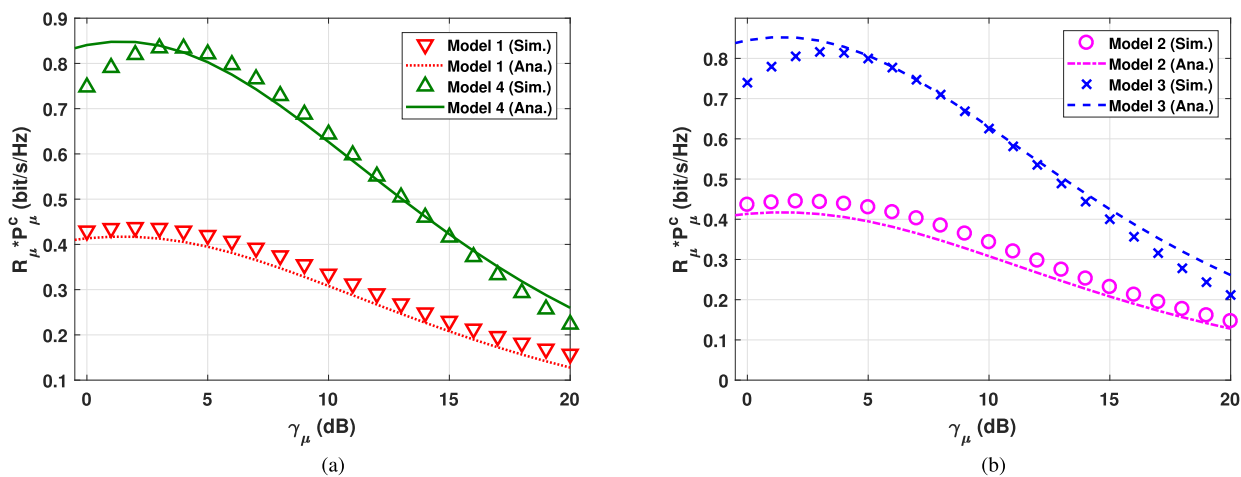**FIGURE 3.** Average rate multiplied by Probability of Coverage ($R_\mu * P_\mu^c$) at different SIR threshold γ_μ. (a) Models 1 and 4. (b) Models 2 and 3.

In Fig. 2b, we show the results for having the directional antenna at FBS (Model 2) and pBSs (Model 3), respectively. As identified before, the coverage probability of Model 1 is closer to Model 2 and Model 3 is close to Model 4.

In Fig. 3, we present a plot for the overall average rate multiplied by the probability of coverage. This metric is considered as the ASE divided by the overall density of the μWave link. Fig. 3 shows a decrease as the required SIR threshold increases, because coverage probability decreases as the SIR threshold increases as shown in Fig. 2. As expected, the results for Models 1 and 2 (3 and 4) are close.

The results of the optimization problem of the ASE and EE for the wireless backhaul μWave tiers discussed in Section III-C1 are presented in Fig. 4. According to the value of β defined in Table 3, and using (23), the analytical optimal SIR threshold $\gamma_\mu^* = 1.3970$ dB for all four models. As mentioned earlier, the slight difference in the simulation

results with respect to analytical results (especially for Models 3 and 4) can be attributed to the way with which the analytical directivity gains was calculated.

B. mmWave TIER
In Fig. 5, we present the results for ASE and EE of mmWave network γ_w. This plot is under the assumption that the distance between the desired pBS and UE is fixed. Although the optimization problem explained in Section III-C2 didn't have a closed form, but the results show the dependence of the optimal SINR on the radius of LOS region. As the radius of the LOS region increases, more pBSs are considered LOS pBSs. This increases which results in a smaller SINR threshold. Thus the curves for $r_w = 150$ m have an optimal SINR threshold smaller than the case of $r_w = 100$ m. There is a slight difference between the simulation and analytical results. This is because of the accuracy of calculating the numerical integrations in (12).
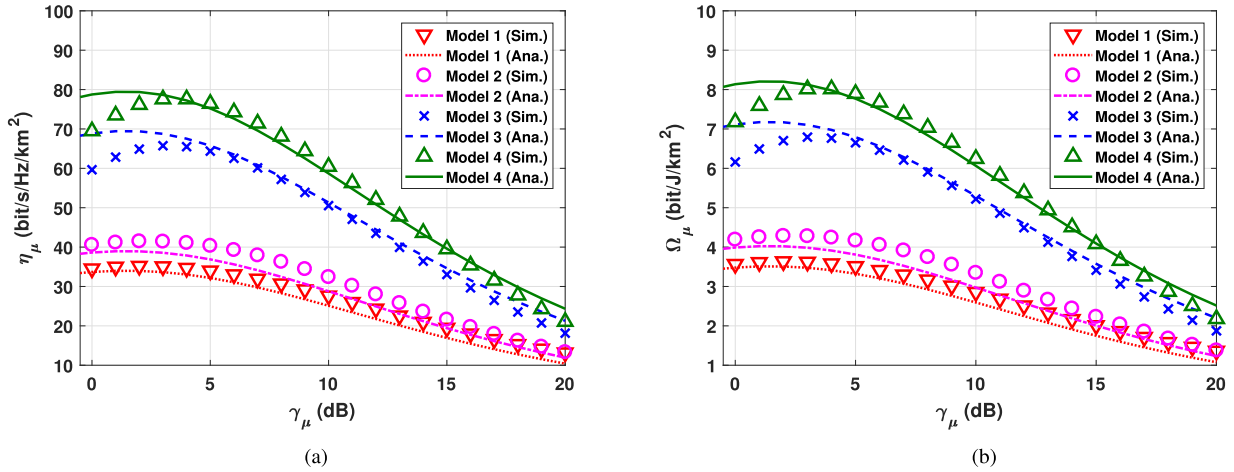
FIGURE 4. μWave link ASE η_μ and EE Ω_μ for different SIR thresholds γ_μ. (a) Area spectral efficiency η_μ. (b) Energy efficiency Ω_μ.
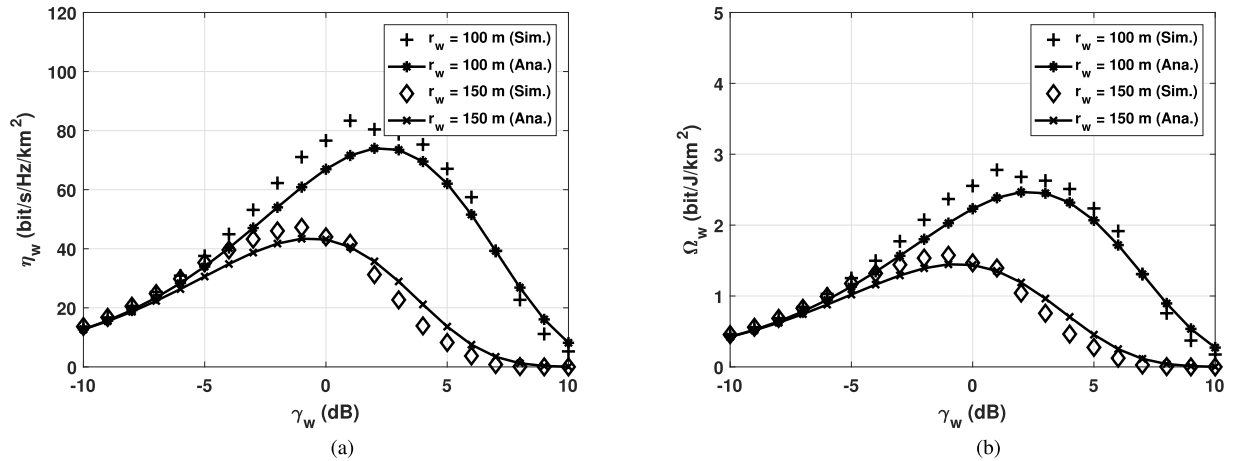

FIGURE 5. mmWave tier area spectral efficiency η_w and energy efficiency Ω_w for different SINR thresholds γ_w. (a) Area spectral efficiency η_w. (b) Energy efficiency Ω_w.

V. ASE AND EE ANALYSIS IN TERMS OF AVERAGE RATE UNDER COVERAGE

In this section, we redo the analysis of the ASE and EE [4] for multi-tier μWave links considering the average rate under coverage instead of the minimum rate model. Please note that this parameter is not the same as the classic ergodic rate, because the rate is calculated conditioned that the typical pBS being in coverage. The average rate under coverage is greater than or equal to minimum average rate and can be analytically computed as

$$R_\mu^c = \log_2(1 + \gamma_{\min}) + \frac{\sum\limits_{j\in\{m,f\}} \lambda_j (P_t^j G_{\max}^j)^{2/\beta} \mathcal{A}(\beta, \gamma_j, \gamma_{\min})}{\sum\limits_{j\in\{m,f\}} \lambda_j (P_t^j G_{\max}^j)^{2/\beta} \gamma_j^{-2/\beta}},$$

(27)

---

[4]Please note that we present the analysis for area spectral efficiency only. This is because both energy and area spectral efficiencies are related by a constant (power consumption) which is independent of the required threshold. However, in the results section we present both metrics.
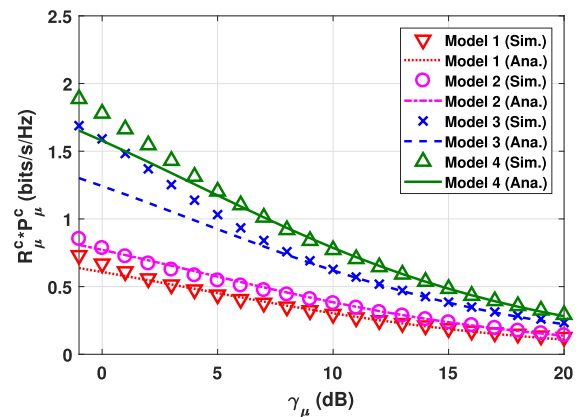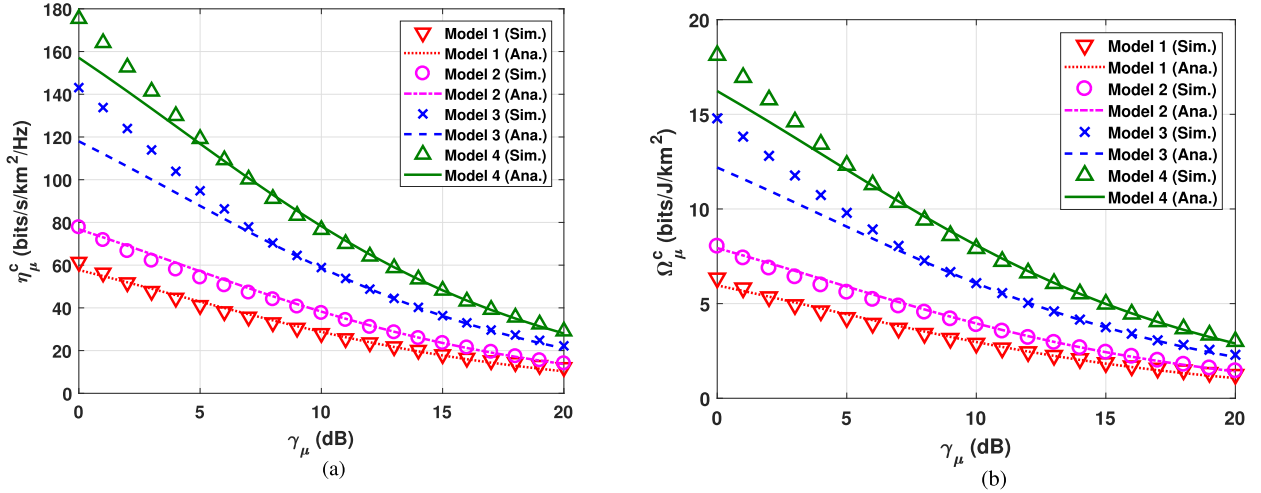

FIGURE 6. μWave rate under coverage multiplied by Probability of Coverage ($R_\mu^c * P_\mu^c$) at different SIR threshold γ_μ.

where $\mathcal{A}(\beta, \gamma_j, \gamma_{\min}) = \int_{\gamma_{\min}}^{\infty} \frac{\max(\gamma_j, x)^{-2/\beta}}{1+x} dx$ and $\gamma_{\min} = \min(\gamma_m, \gamma_f)$. The rest of the notations and definitions are given in Table 1.

FIGURE 7. μWave tier ASE and EE in terms of average rate under coverage for different SIR thresholds γ_μ.

Proof: The proof is similar to the proof of Theorem 2 in [2]. □

The second term in (27) shows that at different thresholds for the multi-tier μWave network, the average rate under coverage is density dependent at different thresholds ($\gamma_f \neq \gamma_m$). As mentioned in Section I-B, since the multi-tier μWave links are deployed as the wireless backhaul, the rate under coverage is required to be separately calculated for μWave link in order to determine its suitability as a reliable wireless backhaul.

The computation of the average rate under coverage for each tier is not as straight forward as the coverage probability. This is due to the split of the constant term $\log_2(1 + \gamma_{\min})$.

Proposition 4: The separated average coverage rate for each tier can be given as

$$R_f^c = \frac{\lambda_f (P_T^f G_{\max}^f)^{2/\beta}}{\sum_{j \in \{m,f\}} \lambda_j (P_T^j G_{\max}^j)^{2/\beta} \gamma_j^{-2/\beta}}$$
$$\times \left[\gamma_f^{-2/\beta} \log_2(1 + \gamma_{min}) + \mathcal{A}(\beta, \gamma_f, \gamma_{\min}) \right], \quad (28a)$$

$$R_m^c = \frac{\lambda_m (P_T^m G_{\max}^m)^{2/\beta}}{\sum_{j \in \{m,f\}} \lambda_j (P_T^j G_{\max}^j)^{2/\beta} \gamma_j^{-2/\beta}}$$
$$\times \left[\gamma_m^{-2/\beta} \log_2(1 + \gamma_{min}) + \mathcal{A}(\beta, \gamma_m, \gamma_{\min}) \right]. \quad (28b)$$

Proof: The proof is given in Appendix C. □

Alternately, these two equations can be re-written with respect to the individual probability of coverage $\mathcal{P}_f^c$, $\mathcal{P}_m^c$ and the total probability of coverage $\mathcal{P}_\mu^c$, as follows

$$R_f^c = \frac{\mathcal{P}_f^c}{\mathcal{P}_\mu^c} \left[\log_2(1 + \gamma_{\min}) + \gamma_f^{2/\beta} \mathcal{A}(\beta, \gamma_f, \gamma_{\min}) \right], \quad (29a)$$

$$R_m^c = \frac{\mathcal{P}_m^c}{\mathcal{P}_\mu^c} \left[\log_2(1 + \gamma_{\min}) + \gamma_m^{2/\beta} \mathcal{A}(\beta, \gamma_m, \gamma_{\min}) \right]. \quad (29b)$$

Although the individual average rates under coverage were derived based on the assumption of different thresholds, we show that this split still holds for same thresholds. This

can be proven by substituting $\gamma_f = \gamma_m = \gamma_\mu$ in (29), which results in

$$R_f^c = \frac{\mathcal{P}_f^c}{\mathcal{P}_\mu^c} \left[\log_2(1 + \gamma_\mu) + \gamma_\mu^{2/\beta} \mathcal{A}(\beta, \gamma_\mu, \gamma_\mu) \right], \quad (30a)$$

$$R_m^c = \frac{\mathcal{P}_m^c}{\mathcal{P}_\mu^c} \left[\log_2(1 + \gamma_\mu) + \gamma_\mu^{2/\beta} \mathcal{A}(\beta, \gamma_\mu, \gamma_\mu) \right]. \quad (30b)$$

A. ASE η_μ^c AND EE Ω_μ^c ANALYSIS

Proposition 5: Under the assumption of $\gamma_j > 1$ [2], ASE and EE are strictly decreasing functions with respect to the threshold, thereby they can be maximized by choosing the lowest possible SIR threshold available in the system.

Proof: To have a comparison between our previous analysis in Section III, we consider the case of same thresholds $\gamma_f = \gamma_m = \gamma_\mu$. Hence, the ASE and EE will be given as:

$$\eta_\mu^c = \left[\lambda_f \mathcal{P}_f^c(\gamma_\mu) + \lambda_m \mathcal{P}_m^c(\gamma_\mu) \right] R_\mu^c(\gamma_\mu), \quad (31a)$$

$$\Omega_\mu^c = \frac{\left[\lambda_f \mathcal{P}_f^c(\gamma_\mu) + \lambda_m \mathcal{P}_m^c(\gamma_\mu) \right] R_\mu^c(\gamma_\mu)}{\sum_{j \in \{m,f\}} \lambda_j (P_{j0} + \Delta_j P_j)}, \quad (31b)$$

where all the parameters are defined previously in Section III and Table 1. By substituting (27) in (31), we obtain

$$\eta_\mu^c = \left[\lambda_f \mathcal{P}_f^c(\gamma_\mu) + \lambda_m \mathcal{P}_m^c(\gamma_\mu) \right]$$
$$\times \left[\log_2(1 + \gamma_\mu) + \gamma_\mu^{2/\beta} \mathcal{A}(\beta, \gamma_\mu, \gamma_\mu) \right]. \quad (32)$$

After simplification, we obtain

$$\eta_\mu^c = \mathcal{C} \left[\gamma_\mu^{-2/\beta} \log_2(1 + \gamma_\mu) + \mathcal{A}(\beta, \gamma_\mu, \gamma_\mu) \right], \quad (33)$$

where $\mathcal{C} = (\lambda_f c_f + \lambda_m c_m)$, and $c_j = \frac{\pi}{C(\beta)} \frac{\lambda_j (P_T^j G_{\max}^j)^{2/\beta}}{\sum_j \lambda_j (P_T^j G_{\min}^j)^{2/\beta}}$, where $j = \{f, m\}$. The rest of the notations are given in Table 1.

The derivative of η_μ^c with respect to γ_μ is given as

$$\partial \eta_\mu^c / \partial \gamma_\mu = -a \gamma_\mu^{-a-1} \log_2(1 + \gamma_\mu), \quad (34)$$

where $a = \frac{2}{\beta}$. Since $\gamma_\mu > 1$, $\partial \eta_\mu^c / \partial \gamma_\mu < 0$. Thus η_μ^c is a decreasing function. $\qquad\square$

B. RESULTS

In this subsection, we present the results of the average rate under coverage multiplied by coverage probability, ASE and EE in terms of average rate under coverage. The results show that ASE and EE are decreasing function for $\gamma_\mu > 1$.

In Fig. 6, we present a plot for the overall average rate under coverage multiplied by the probability of coverage. This metric is considered as the average rate achievable by a random pBSs when it is in coverage. Fig. 6 shows a decrease as the SIR threshold increases, because coverage probability decreases as the threshold increases as shown in Fig. 2. As identified before, the way in which the analytical gain of ESPAR antenna was calculated might have resulted in the slight difference in the simulation results with respect to analytical results (especially for Models 3 and 4).

The coverage probability is the key parameter for calculating the ASE and EE. Therefore, we expect the same behaviour in Figures 2 and 6 for Fig. 7. ASE and EE results presented in Fig. 7 are considering the average rate under coverage. According to Proposition 5, the maximum ASE and EE oocurs at $\gamma_\mu = 0$ dB. From these results, we conclude that the performance of the μWave tiers as wireless backhaul can be improved by exploiting directional antennas. This improvement depends on the placement of directional antenna on the transmitter and/or receiver. Moreover, the results in Figures 6 and 7 confirm what we stated in Proposition 5.

VI. CONCLUSION

In this paper, we considered a three-tier hybrid cellular heterogeneous network (HetNet) using microwave (μWave) links for the first two tiers and millimeter (mmWave) links for the last tier. The μWave links were used as wireless backhaul to the last tier with mmWave links. It was assumed that the end-user could only connect to the last tier. Because the main challenge in having a wireless backhaul is mitigating interference, we proposed a novel and practical model where we reuse the μWave infrastructure, and equip the BSs with directional antennas to have a robust wireless backhaul network. Moreover, equipping the μWave tiers with directional antennas showed an improvement in the performance metrics, such as, coverage probability, average rate under coverage, ASE and EE. Furthermore, different placements for the directional antennas were presented, in order to have a robust wireless backhaul as well as an overall low system complexity. We studied an optimization problem for the overall area spectral and energy efficiency with respect to the optimal Signal-to-Interference ratio (SIR) threshold for μWave and mmWave links in terms of minimum rate model. The results indicated that the optimal threshold required for the μWave tiers (wireless backhaul) depends on the path-loss exponent and that for the mmWave tier depended on the area of line-of-sight (LOS) region. Furthermore, we studied the average rate under coverage, and its effect on ASE and EE. We proved

that using the average rate under coverage model, the optimal threshold is the minimum, as ASE and EE are strictly decreasing functions. We conclude that the proposed hybrid HetNet model with μWave links as the wireless backhaul and mmWave based end-users can be made practically feasible for deployment with the appropriate choice/placement of directional antennas and with suitable setting of thresholds at different tiers.

APPENDIX A
PROOF OF PROPOSITION 1

Proof: The coverage probability in a K-tier wireless backhaul network under instantaneous SIR based scheme for directional antennas equipped at FBSs and typical pBS can be derived as follows:

$$
\begin{aligned}
P_c &\overset{(a)}{=} \sum_{i=1}^{K} \mathbf{E}\left[\sum_{x_i \in \Phi_i} \mathbf{1}\left(SIR(x_i) > \theta_i \right) \right] \\
&\overset{(b)}{=} \sum_{i=1}^{K} \lambda_i \int_{\mathbb{R}^2} \mathbf{P}\left(\frac{P_T^i G_{\max}^i |h_0^i|^2 x_i^{-\beta}}{I_{x_i}} > \theta_i \right) dx_i, \\
&\overset{(c)}{=} \sum_{i=1}^{K} \lambda_i \int_{\mathbb{R}^2} \mathcal{L}_{I_i}\left(\frac{\theta_i x^\beta}{P_T G_{\max}^i} \right) dx_i,
\end{aligned}
\tag{35}
$$

(a) follows Lemma 1 [2] under the assumption that $\theta_i > 1$, (b) follows Campbell Mecke Theorem [43], and (c) follows the assumption of Rayleigh distributed channel coefficients. Since the point processes are stationary, the interference is independent of the location of the nodes. Thus, the total interference $I_{\text{total}} = \sum_{i=1}^{K} I_{x \in \Phi_i}$, where $I_i = \sum_{j \in \Phi_j} P_j G_{\text{int}_j} |h_j|^2 x_j^{-\beta}$ for $i = (1, 2, 3...K)$. Then, $\mathcal{L}_{I_i}(s)$ is given by.

$$
\begin{aligned}
\mathcal{L}_{I_i}(s) &= \prod_{j=1}^{K} \mathop{\mathbf{E}}_{\Phi_j}\left[\prod_{j \in \Phi_j} \mathbf{E}_h \exp\left(-s\epsilon x^\beta P_T^j G_{\text{int}}^j |h_j|^2 x_j^{-\beta} \right) \right] \\
&\overset{(a)}{=} \prod_{j=1}^{K} \mathop{\mathbf{E}}_{\Phi_j}\left[\prod_{j \in \Phi_j} \frac{1}{\left(1 + s\rho x_j^{-\beta} \right)} \right] \\
&\overset{(b)}{=} \prod_{j=1}^{K} \exp\left(-2\pi \lambda_j p_j \int_0^\infty \left(1 - \frac{1}{\left(1 + s\rho x_j^{-\beta} \right)} \right) dx_j \right)
\end{aligned}
\tag{36}
$$

where $\rho = \epsilon x^\beta P_T^j G_{\text{int}}^j$, $\epsilon = \theta_i / P_T^j G_{\max}^j$, (a) follows the Rayleigh fading assumption, and (b) follows from probability generating function (PGFL) of PPP [27]. By substituting (36) in (35) and under the assumption of Rayleigh fading and neglecting the noise, a closed form expression for the total coverage probability is given in (7).

This concludes the proof. $\qquad\square$

APPENDIX B
PROOF OF PROPOSITION 2

Proof: The mmWave typical user is always connected to the desired mmWave pBS with the highest SINR. The desired

mmWave pBS can be located either in the LOS or NLOS regions. The LOS region is denoted as a circle surrounding the mmWave UE with a certain radius r. If the mmWave pBS is within this circle, then it is a LOS mmWave pBS. If this circle is empty, (i.e. there is no mmWave pBS in it), then the desired mmWave pBS is a NLOS pBS. We consider the PPP of the mmWave pBSs divided into two tier network with same threshold γ_w, consisting of the LOS PPP (Φ_L) with intensity λp_L and NLOS PPP (Φ_N) with intensity λp_N. These two marked PPPs are homogeneous due to the assumption of fixed LOS probability. Therefore the coverage probability can be written as

$$
\begin{aligned}
P_w^c &= \sum_{z \in \{L,N\}} \mathbf{E}\left[\mathbf{1}(SINR_z > \gamma_w)\right], \\
&= \sum_{z \in \{L,N\}} \int_{\mathbb{R}^2} \mathbf{P}\left(\frac{P_T^w G_{\max} |g_0|^2 x_z^{-\alpha_z}}{\sigma^2 + I_z} > \gamma_w \right) dx_z \\
&= \sum_{z \in \{L,N\}} \int_{\mathbb{R}^2} \mathbf{P}\left(|g_0|^2 > \frac{\gamma_w x_z^{\alpha_z}\left(\sigma^2 + I\right)}{P_T^w G_{\max}} \right) dx_z \quad (37)
\end{aligned}
$$

Since the mmWave channel experience Rayleigh fading, the channel gain is exponentially distributed. Therefore, (37) becomes

$$
P_w^c = \sum_{z \in \{L,N\}} e^{-\frac{\gamma_w x_z^{\alpha_z}\sigma^2}{P_T^w G_{\max}}} \mathop{\mathbf{E}}_{x_z \in \Phi_z}\left[e^{-\frac{\gamma_w x_z^{\alpha_z} I_z}{P_T^w G_{\max}}} \right], \quad (38)
$$

where the total interference I is the sum of the interference from LOS and NLOS mmWave pBSs given as

$$
I = \sum_{l \in \Phi_L} P_T^w G_{int_l}^w |h_l^w|^2 y_l^{-\alpha_L} + \sum_{n \in \Phi_N} P_T^w G_{int_n}^w |h_n^w|^2 y_n^{-\alpha_N}. \quad (39)
$$

By substituting in (38) using (39), and using the stochastic geometry steps similar to the HetNet case, (10) is obtained.

This concludes the proof. $\qquad\square$

APPENDIX C
PROOF OF PROPOSITION 4

Proof: Given the HetNet average coverage rate as

$$
\begin{aligned}
\bar{R}_H = \log(1 + \gamma_{\min}) \\
+ \frac{\sum\limits_{j \in \{m,f\}} \lambda_j (P_T^j G_{\min}^j)^{2/\alpha} \mathcal{A}(\alpha, \gamma_j, \gamma_{\min})}{\sum\limits_{j \in \{m,f\}} \lambda_j (P_T^j G_{\max}^j)^{2/\alpha} \gamma_j^{-2/\alpha}}, \quad (40)
\end{aligned}
$$

where $\mathcal{A}(\alpha, \gamma_j, \gamma_{\min}) = \int_{\gamma_{\min}}^{\infty} \frac{\max(\gamma_j, x)^{-2/\alpha}}{1 + x} dx$.

Since $\mathcal{P}_f^c + \mathcal{P}_m^c = \mathcal{P}_\mu^c$, $\frac{\mathcal{P}_f^c + \mathcal{P}_m^c}{\mathcal{P}_\mu^c} = 1$. The first term in (27) can be written as

$$
\log(1 + \gamma_{\min}) = \frac{\mathcal{P}_f^c \log(1 + \gamma_{\min})}{\mathcal{P}_\mu^c} + \frac{\mathcal{P}_m^c \log(1 + \gamma_{\min})}{\mathcal{P}_\mu^c} \quad (41)
$$

By substituting equation (7) of $\mathcal{P}_\mu^c$, and equations (9a) of $\mathcal{P}_f^c$, $\mathcal{P}_m^c$, respectively, in (41), the first term in equations (28a) and (28b) is obtained. The second term in (27) can be divided into two independent parts for the 2 tier following the same assumption as in Remark 1. Therefore, (27) can be splitted into (28a) and (28b).

This concludes the proof. $\qquad\square$

REFERENCES

[1] C. Li, J. Zhang, J. G. Andrews, and K. B. Letaief, "Success probability and area spectral efficiency in multiuser MIMO HetNets," *IEEE Trans. Commun.*, vol. 64, no. 4, pp. 1544–1556, Apr. 2016.

[2] H. S. Dhillon, R. K. Ganti, F. Baccelli, and J. G. Andrews, "Modeling and analysis of K-tier downlink heterogeneous cellular networks," *IEEE J. Sel. Areas Commun.*, vol. 30, no. 3, pp. 550–560, Apr. 2012.

[3] H. Wang, S.-H. Leung, and R. Song, "Uplink area spectral efficiency analysis for multichannel heterogeneous cellular networks with interference coordination," *IEEE Access*, vol. 6, pp. 14485–14497, 2018.

[4] Y. S. Soh, T. Q. S. Quek, M. Kountouris, and H. Shin, "Energy efficient heterogeneous cellular networks," *IEEE J. Sel. Areas Commun.*, vol. 31, no. 5, pp. 840–850, May 2013.

[5] H.-S. Jo, Y. J. Sang, P. Xia, and J. G. Andrews, "Heterogeneous cellular networks with flexible cell association: A comprehensive downlink SINR analysis," *IEEE Trans. Wireless Commun.*, vol. 11, no. 10, pp. 3484–3495, Oct. 2012.

[6] H. Elsawy, E. Hossain, and M. Haenggi, "Stochastic geometry for modeling, analysis, and design of multi-tier and cognitive cellular wireless networks: A survey," *IEEE Commun. Surveys Tuts.*, vol. 15, no. 3, pp. 996–1019, Jun. 2013.

[7] Y. Hao, B. Ni, H. Li, and S. Hou, "On the energy and spectral efficiency tradeoff in massive MIMO-enabled HetNets with capacity-constrained backhaul links," *IEEE Trans. Commun.*, vol. 65, no. 11, pp. 4720–4733, Nov. 2017.

[8] M. Xiao *et al.*, "Millimeter wave communications for future mobile networks," *IEEE J. Sel. Areas Commun.*, vol. 35, no. 9, pp. 1909–1935, Sep. 2017.

[9] X. Ge, B. Yang, J. Ye, G. Mao, C.-X. Wang, and T. Han, "Spatial spectrum and energy efficiency of random cellular networks," *IEEE Trans. Commun.*, vol. 63, no. 3, pp. 1019–1030, Mar. 2015.

[10] T. S. Rappaport *et al.*, "Millimeter wave mobile communications for 5G cellular: It will work!" *IEEE Access*, vol. 1, pp. 335–349, May 2013.

[11] T. Bai and R. W. Heath, Jr., "Coverage and rate analysis for millimeter-wave cellular networks," *IEEE Trans. Wireless Commun.*, vol. 14, no. 2, pp. 1100–1114, Feb. 2015.

[12] S. Singh, M. N. Kulkarni, and J. G. Andrews, "A tractable model for rate in noise limited mmWave cellular networks," in *Proc. 48th Asilomar Conf. Signals, Syst. Comput.*, Nov. 2014, pp. 1911–1915.

[13] R. W. Heath, Jr., N. González-Prelcic, S. Rangan, W. Roh, and A. M. Sayeed, "An overview of signal processing techniques for millimeter wave MIMO systems," *IEEE J. Sel. Topics Signal Process.*, vol. 10, no. 3, pp. 436–453, Apr. 2016.

[14] M. S. Omar, M. A. Anjum, S. A. Hassan, H. Pervaiz, and Q. Niv, "Performance analysis of hybrid 5G cellular networks exploiting mmwave capabilities in suburban areas," in *Proc. IEEE Int. Conf. Commun. (ICC)*, May 2016, pp. 1–6.

[15] A. Umer, S. A. Hassan, H. Pervaiz, Q. Ni, and L. Musavian, "Coverage and rate analysis for massive MIMO-enabled heterogeneous networks with millimeter wave small cells," in *Proc. IEEE 85th Veh. Technol. Conf. (VTC Spring)*, Jun. 2017, pp. 1–5.

[16] M. S. Omar *et al.*, "Multiobjective optimization in 5G hybrid networks," *IEEE Internet Things J.*, vol. 5, no. 3, pp. 1588–1597, Jun. 2018.

[17] U. Siddique, H. Tabassum, E. Hossain, and D. I. Kim, "Wireless backhauling of 5G small cells: Challenges and solution approaches," *IEEE Wireless Commun.*, vol. 22, no. 5, pp. 22–31, Oct. 2015.

[18] J. Zhao, T. Q. S. Quek, and Z. Lei, "Heterogeneous cellular networks using wireless backhaul: Fast admission control and large system analysis," *IEEE J. Sel. Areas Commun.*, vol. 33, no. 10, pp. 2128–2143, Oct. 2015.

[19] N. Wang, E. Hossain, and V. K. Bhargava, "Joint downlink cell association and bandwidth allocation for wireless backhauling in two-tier HetNets with large-scale antenna arrays," *IEEE Trans. Wireless Commun.*, vol. 15, no. 5, pp. 3251–3268, May 2016.

[20] P. Huang and K. Psounis, "Efficient mmWave wireless backhauling for dense small-cell deployments," in *Proc. 13th Annu. Conf. Wireless On-Demand Netw. Syst. Services (WONS)*, Feb. 2017, pp. 88–95.

[21] E. Zola, A. J. Kassler, and W. Kim, "Joint user association and energy aware routing for green small cell mmWave backhaul networks," in *Proc. IEEE Wireless Commun. Netw. Conf. (WCNC)*, Mar. 2017, pp. 1–6.

[22] Z. Su *et al.*, "User association and wireless backhaul bandwidth allocation for 5G heterogeneous networks in the millimeter-wave band," *China Commun.*, vol. 15, no. 4, pp. 1–13, Apr. 2018.

[23] T. M. Nguyen, W. Ajib, and C. Assi, "Designing wireless backhaul heterogeneous networks with small cell buffering," *IEEE Trans. Commun.*, vol. 66, no. 10, pp. 4596–4610, Oct. 2018.

[24] U. Siddique, H. Tabassum, and E. Hossain, "Downlink spectrum allocation for in-band and out-band wireless backhauling of full-duplex small cells," *IEEE Trans. Commun.*, vol. 65, no. 8, pp. 3538–3554, Aug. 2017.

[25] S. Singh, M. N. Kulkarni, A. Ghosh, and J. G. Andrews, "Tractable model for rate in self-backhauled millimeter wave cellular networks," *IEEE J. Sel. Areas Commun.*, vol. 33, no. 10, pp. 2196–2211, Oct. 2015.

[26] J. Zhao, S. Zhao, H. Qu, and G. Ren, "Modeling and analyzing multi-tier millimeter/micro wave hybrid caching networks," *IEEE Access*, vol. 6, pp. 52703–52712, 2018.

[27] D. Stoyan, W. D. Kendall, and J. Mecke, *Stochastic Geometry and Its Applications*, 2nd ed. Hoboken, NJ, USA: Wiley, 2008.

[28] F. Baccelli and B. Blaszczyszyn, *Stochastic Geometry and Wireless Networks: Applications*, vol. 2. Norwell, MA, USA: NOW, 2009.

[29] B. Khamidehi and M. Sabbaghian, "Resource allocation for SC-FDMA femtocell networks," *IEEE Trans. Veh. Technol.*, to be published, doi: 10.1109/TVT.2017.2751077.

[30] O. Y. Kolawole, S. Vuppala, and T. Ratnarajah, "Multiuser millimeter wave cloud radio access networks with hybrid precoding," *IEEE Syst. J.*, vol. 12, no. 4, pp. 3661–3672, Dec. 2018.

[31] J. G. Andrews, F. Baccelli, and R. K. Ganti, "A tractable approach to coverage and rate in cellular networks," *IEEE Trans. Commun.*, vol. 59, no. 11, pp. 3122–3134, Nov. 2011.

[32] R. F. Rudd and M. Nekovee, "Millimetre-wave propagation in urban clutter for 5G systems," in *Proc. Loughborough Antennas Propag. Conf. (LAPC)*, Nov. 2017, pp. 1–2.

[33] M. Di Renzo, A. Guidotti, and G. E. Corazza, "Average rate of downlink heterogeneous cellular networks over generalized fading channels: A stochastic geometry approach," *IEEE Trans. Commun.*, vol. 61, no. 7, pp. 3050–3071, Jul. 2013.

[34] E. Turgut and M. C. Gursoy, "Energy efficiency in relay-assisted mmWave cellular networks," in *Proc. IEEE 84th Veh. Technol. Conf. (VTC-Fall)*, Sep. 2016, pp. 1–5.

[35] S. Boyd and L. Vandenberghe, *Convex Optimization*. Cambridge, U.K.: Cambridge Univ. Press, 2004.

[36] A. Abdalrazik, H. Soliman, M. F. Abdelkader, and T. M. Abuelfadl, "Power performance enhancement of underlay spectrum sharing using microstrip patch ESPAR antenna," in *Proc. IEEE Wireless Commun. Netw. Conf.*, Apr. 2016, pp. 1–6.

[37] E. P. Tsakalaki, D. Wilcox, E. de Carvalho, C. B. Papadias, and T. Ratnarajah, "Spectrum sensing using single-radio switched-beam antenna systems," in *Proc. 7th Int. ICST Conf. Cognit. Radio Oriented Wireless Netw. Commun. (CROWNCOM)*, Jun. 2012, pp. 118–123.

[38] D. Wilcox, E. Tsakalaki, A. Kortun, T. Ratnarajah, C. B. Papadias, and M. Sellathurai, "On spatial domain cognitive radio using single-radio parasitic antenna arrays," *IEEE J. Sel. Areas Commun.*, vol. 31, no. 3, pp. 571–580, Mar. 2013.

[39] A. Kausar, H. Mehrpouyan, M. Sellathurai, R. Qian, and S. Kausar, "Energy efficient switched parasitic array antenna for 5G networks and IoT," in *Proc. Loughborough Antennas Propag. Conf. (LAPC)*, Nov. 2016, pp. 1–5.

[40] R. Qian and M. Sellathurai, "Interference mitigation in femtocell networks using single-radio parasitic antennas," in *Proc. IEEE Int. Conf. Commun.*, Jun. 2015, pp. 2828–2833.

[41] H. Shoukry, R. Qian, and M. Sellathurai, "Performance analysis in indoor femtocell networks using ESPAR antennas," in *Proc. IEEE 17th Int. Workshop Signal Process. Adv. Wireless Commun. (SPAWC)*, Jul. 2, pp. 1–5.

[42] M. Rzymowski, P. Woznica, and L. Kulas, "Single-anchor indoor localization using ESPAR antenna," *IEEE Antennas Wireless Propag. Lett.*, vol. 15, pp. 1183–1186, 2016.

[43] D. Stoyan, W. Kendall, and J. Mecke, *Stochastic Geometry and Its Applications*, 2nd ed. Hoboken, NJ, USA: Wiley, 1996.

HEBATALLAH SHOUKRY was born in Alexandria, Egypt, in 1983. She received the B.Sc. degree (Hons.) in electrical engineering from the Communication Department, Alexandria University, Egypt, in 2006, and the two M.Sc. degrees in electrical engineering from the University of Central Florida, Orlando, FL, USA, and Friedrich-Alexander University, Erlangen, Germany, in 2010 and 2013, respectively. She is currently pursuing the Ph.D. degree with Heriot-Watt University, U.K. She was a Research Assistant with Friedrich-Alexander University, from 2013 to 2014. Her current research interests include stochastic geometry, analysis of wireless cellular networks, and ad-hoc sensor networks.

NAVEEN MYSORE BALASUBRAMANYA received the M.S. degree in electrical engineering from the University of Colorado Boulder, Boulder, USA, in 2010, and the Ph.D. degree in electrical and computer engineering from The University of British Columbia, Vancouver, BC, Canada, in 2017. He has more than seven years of academic and industrial research and development industry experience, he was a Postdoctoral Research Associate with Heriot-Watt University, Edinburgh, U.K., and as a Senior Design Engineer for ADSL, WiMAX, and LTE Systems in leading communication industries, such as Lantiq Communications (Intel) India Pvt., Ltd., Broadcom Communications India Pvt., Ltd., and Tata Elxsi Ltd., Bangalore, India. Since 2018, he has been an Assistant Professor with IIT Dharwad, Dharwad, India. His research interests include theory and practical aspects of wireless communications, with a focus on machine-to-machine communication, and the energy efficient Internet of Things.

SATYANARAYANA VUPPALA (S'12–M'17) received the B.Tech. degree (Hons.) in computer science and engineering from Jawaharlal Nehru Technological University at Kakinada, Kakinada, India, in 2009, the M.Tech. degree in information security from the National Institute of Technology, Durgapur, India, in 2011, and the Ph.D. degree in electrical engineering from Jacobs University Bremen, in 2015. He was a Postdoctoral Researcher with the Interdisciplinary Centre for Security, Reliability and Trust, University of Luxembourg. He is currently a Senior Research Scientist with the United Technologies Research Center, Ireland. He also works on physical, access, and network layer aspects of wireless security. He has authored more than 50 publications in refereed international journals and conferences. His research interests include cyber physical security, the Internet of Things, content delivery networks, and wireless communications with particular focus on 5G.

MATHINI SELLATHURAI (SM'06) has made seminal contributions on MIMO wireless systems. She is currently a Full Professor in signal processing and intelligent systems with Heriot-Watt University, Edinburgh, U.K., in her 15-year research on signal processing for communications. She has published 200 IEEE entries with more than 2300 citations, given invited talks and has written a book and several book chapters in topics related to this project. She is also a member for IEEE SPCOM Technical Strategy Committee. She was a recipient of the Best Ph.D. Thesis Award (Silver Medal) from NSERC Canada, in 2002, the IEEE Communications Society Fred W. Ellersick Best Paper Award, in 2005, and the Industry Canada Public Service Awards for contributions in Science and Technology, in 2005. She is the General Co-Chair of IEEE SPAWC2016, Edinburgh. She was an Editor of the IEEE TRANSACTIONS ON SIGNAL PROCESSING from 2009 to 2014. She is currently serving as an IEEE SPCOM Technical Committee Member.